Electrical effective parameters of the grains and the Montgomery's method in $$\hbox {Bi}_{1.65}\hbox {Pb}_{0.35}\hbox {Sr}_2\hbox {Ca}_{2.5}\hbox {Cu}_{3.5}\hbox {O}_y$$ Bi1.65Pb0.35Sr2Ca2.5Cu3.5Oy ceramics

A. Cruz-García, J. R. Fernández-Gamboa, E. Altshuler, R. F. Jardim, O. Vazquez-Robaina, et al.

Journal of Materials Science: Materials in Electronics

ISSN 0957-4522

J Mater Sci: Mater Electron
DOI 10.1007/s10854-018-9566-2

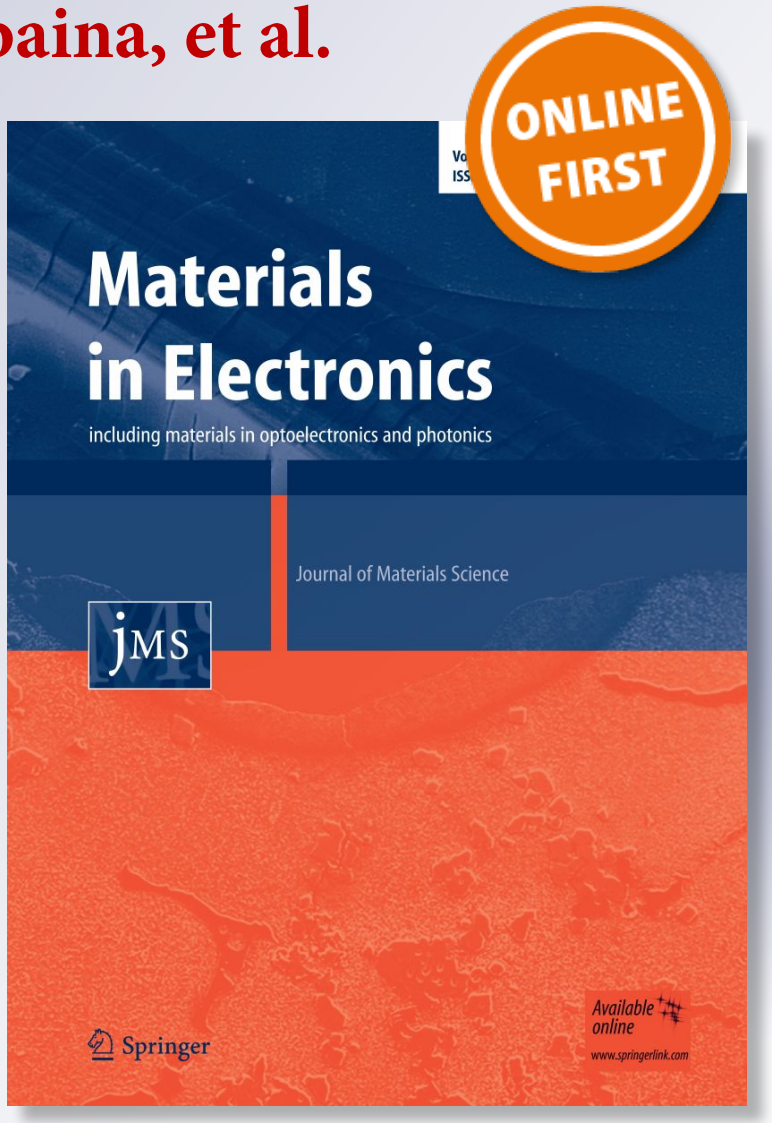

Springer

Journal of Materials Science: Materials in Electronics
https://doi.org/10.1007/s10854-018-9566-2

Electrical effective parameters of the grains and the Montgomery's method in $Bi_{1.65}Pb_{0.35}Sr_2Ca_{2.5}Cu_{3.5}O_y$ ceramics

A. Cruz-García[1] · J. R. Fernández-Gamboa[1] · E. Altshuler[2] · R. F. Jardim[3] · O. Vazquez-Robaina[4] · P. Muné[1]

Received: 28 May 2018 / Accepted: 26 June 2018

Abstract
In this paper we have applied the Montgomery's measurement method to $Bi_{1.65}Pb_{0.35}Sr_2Ca_{2.5}Cu_{3.5}O_y$ ceramic samples, to study the behavior of the grains' electrical effective parameters, such as: intrinsic effective anisotropy, $t = \rho_c/\rho_{ab}$, the slope of the linear part in the temperature dependence of the ab-planes resistivity, $A_{ab} = \Delta\rho_{ab}/\Delta T$, the weak links resistivity, ρ_{wl}, and the orientation probability of the grains' a-axes along a certain preferential direction, γ_{xa}. Here, ρ_{ab}, ρ_c and T are the main values of the resistivitity tensor and the measurement temperature, respectively. The samples were pressed uniaxially at three different compacting pressures and extracted from the pellets by cutting an slab along the cylinder axis. Samples cut in this way, exhibit almost an isotropic behavior in the transport properties. Moreover, the sample extracted from the pellet compacted at 488 MPa exhibits the best inter and intragranular properties. The effective intrinsic anisotropy of its grains has the lowest value in the sample set. These results can be used in the fabrication of this superconducting material for certain applications.

1 Introduction

$(BiPb)_2Sr_2Ca_2Cu_3O_{10+\delta}$ ((Bi,Pb)2223) ceramic samples extracted from different regions of the same pellet show an inhomogeneous distribution of microstructural properties [1]. It may be observed by means of electrical transport measurements in low applied magnetic fields. In particular, samples extracted from regions of the pellet near the face where the piston used for sample the compaction has a direct mechanical contact with the powders, or near the opposite face of the pellet, exhibit a better intergranular connectivity, grain alignment and transport properties than samples extracted from regions near the core of the cylindrical pellet [1]. On the other hand, (Bi,Pb)2223 ceramic samples are, on the whole, anisotropic due to the great intrinsic and shape anisotropy of their grains.

Various measuring methods have been developed to obtain separately the resistivity tensor components ($[\hat{\rho}_e]_{ii} = \rho_i$ with $i = x, y, z$ respectively). The most commonly used is the so-called Montgomery's method [2] which is based in other previous works on the subject [3–5]. To apply this method in single crystals, the sample is shaped into a rectangular block, the faces of which are orthogonal to the principal crystallographic axes. Current is applied through the contacts on two corners of one planar face of the crystal, and the contacts located on the other two corners of the same plane allow recording the voltage. A similar measurement is then performed with the electrical connections rotated by 90° (see Fig. 1). Two components of the electrical resistivity tensor may be calculated from these measurements and the dimensions of the sample. If the determination of the third tensor component is required, measurements on another face of the crystal are needed [2, 3, 5, 6].

Recently, electric transport properties were studied in (Bi,Pb)2223 polycrystalline samples that were cut from the upper or lower surfaces of cylindrical pellet [7]. Under these conditions, it was possible to determine the effective

✉ P. Muné
mune@uo.edu.cu

A. Cruz-García
acruz@uo.edu.cu

1 Departamento de Física, Universidad de Oriente, P. Lumumba s/n, 90500 Santiago de Cuba, Cuba

2 Superconductivity Laboratory and Group of Complex Systems and Statistical Physics, IMRE-Physics Faculty, University of Havana, 10400 Havana, Cuba

3 Departamento de Física dos Materiais e Mecânica, Instituto de Física, Universidade de São Paulo, CP 66318, São Paulo, SP 05315-970, Brazil

4 LIEES Department, IMRE-Physics Faculty, University of Havana, 10400 Havana, Cuba

Published online: 04 July 2018

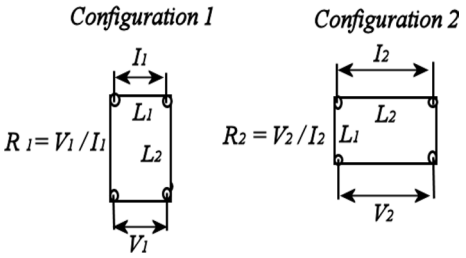

Fig. 1 Contact configurations for an anisotropic sample using the Montgomery method. V_1 and V_2 are the voltages measured as a result of the applied electrical currents I_1 in configuration 1 and I_2 in configuration 2, respectively

anisotropy at sample level, $\mu = \rho_z/\rho_x$, which resulted to be ($\mu \geq 18$) [7]. Afterwards, by using an effective medium approximation model applied to electric transport measurements of the polycrystals [7, 8], the effective anisotropy of the grains [7], $t = \rho_c/\rho_{ab}$, their orientation probability, γ_{xa}, the weak links resistivity, ρ_{wl}, and the slope of the temperature dependence of the grains' resistivity, $A_{ab} = \Delta\rho_{ab}/\Delta T$ were determined. Here, ρ_c, ρ_{ab} and T are the out-of-plane resistivity, the in-plane resistivity and the temperature of the samples, respectively [7]. These recent results for superconducting polycrystalline samples, show that high pelletization pressures affect not only the intergranular, but also the intragranular transport properties by increasing the density of defects and reducing the effective anisotropy of the grains [7].

In this paper we have applied the model developed in reference [7] to $\rho(T)$ measurements obtained by means of the Montgomery's method in $Bi_{1.65}Pb_{0.35}Sr_2Ca_{2.5}Cu_{3.5}O_y$ samples with very low anisotropy. Similar behavior of the intragranular properties were obtained by using a different measure method in samples with higher anisotropy [9], but with the same starting composition used here. Thus, the results that will be presented here are an experimental contribution to the verification of the model described in reference [7] for samples with low anisotropy.

2 Experimental details

Samples examined in this paper were sintered by using as starting compounds: Bi_2O_3 (99%), PbO (99%), $SrCO_3$ (99%), $CaCO_3$ (99%), and CuO (99%) with the atomic ratios of Pb:Bi:Sr:Ca:Cu (0.35:1.65:2:2.5:3.5). These powders were weighed, mixed thoroughly by hand under isopropanol using an agate mortar and pestle. Other details about the obtaining process, which includes heat treatments at different temperatures for 40 h followed of sequential grounds and pelletizations, can be found elsewhere [9–11]. In this case, the compacting pressures of each pellet before the last heat treatment, the dimensions of the sintered pellets and their mass are given in Table 1. The sintering temperature was 826 °C.

The densities of the three samples were determined by ratio of mass to volume. The volumes were measured from the same cylindric shape of the samples and their dimensions were determined with a resolution of 0.05 mm. The masses were measured with 0.1 mg of resolution. After that, the volume fraction of pores and no conductive phases, p, was estimated starting from the resulting density and the structural one [9, 12, 13].

The microstructure was observed by means of scanning electron microscopy (SEM) in the fractured surfaces of the samples. The micrographies was performed with a microscope model Hitachi S-530, which has nominal resolution of ~ 30–40 nm operating within an interval of 15–20 kV. The platelet shape of the grains is revealed in all samples.

By using a Bruker-AXS D8 Advance X-ray diffractometer, we have identified the crystallographic phases in the powders before the last heat treatment. The patterns were taken at room temperature using Cu Kα radiation in the $3 \leq 2\theta \leq 60$ range with a 0.05° (2θ) step size and 100 s per step.

In order to measure the temperature dependence of the electrical resistivity tensor and its components in the para-coherent state, the samples were cut from the pellets in slab form, as showed in Fig. 2. The dimensions of the three cut samples are displayed in Table 2. Electrical contacts were prepared using silver paint with a heat treatment at 730 °C for 20 min, these were as small as possible in order to minimize their effects on the voltage measurements. The typical contact size was about 5% of the block dimensions.

Table 1 Uniaxial compacting pressures, cylinder shape dimensions and mass of the samples

Sample	Pressure (MPa)	Diameter (mm)	Thickness (mm)	Mass (g)
MD2P1	293	8	2.75	0.6363
MD2P2	488	8	3.2	0.8015
MD2P3	780	8	2.6	0.6805

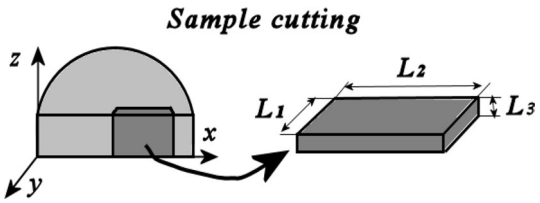

Fig. 2 Sample cutting to be measured by the Montgomery's method

Table 2 Dimensions of the samples

Sample	Length (cm)	Width (cm)	Thickness (cm)
MD2P1	0.349	0.270	0.060
MD2P2	0.349	0.260	0.050
MD2P3	0.379	0.259	0.060

Before each measurement, the samples were cooled from room temperature down to ≈ 80 K. The excitation current was injected according to the Montgomery's method [2, 6]. Both the voltage across the sample and its temperature were collected while the temperature was raised slowly to 300 K for the case of the temperature dependence of the electrical resistivity tensor.

Current–voltage (I–V) measurements were performed in order to determine the resistivity tensor components in the paracoherent state [9]. In this experiment, we have used the Montgomery's technique, as described elsewhere [6]. Once the sample was cooled down and fixed at a given temperature close to 103 K, the I–V curve was taken. From the results, ρ versus J curves are built and paracoherent resistivity tensor component was determined by taking the resistivity value at the point where the slope of the ρ–J curve starts to decrease. This way, we are avoiding the "contamination" of the measurements due to the presence of intragranular dissipation sources [7, 8].

In both types of measurements described before, four electrical contacts were placed on the upper face of the samples according to the Montgomery's method showed in Fig. 1 and described in reference [6].

The diagram displayed in Fig. 2 of the references [7, 9] sketches the procedure to get the inter and intragranular magnitudes starting from the transport measurements described above.

3 Results and discussion

3.1 Micro-structural analysis and X-ray diffraction patterns

The relative volume fractions of the high-T_c (Bi,Pb)2223 phase, f_H, is calculated based on the following equation [14–16]:

$$f_H = \frac{\Sigma I_{H(hkl)}}{\Sigma I_{H(hkl)} + \Sigma I_{L(hkl)} + \Sigma I_{E_1(hkl)}} \quad (1)$$

Here, $I_{H(hkl)}$, $I_{L(hkl)}$ and $I_{E_1(hkl)}$ are the intensities of the (hkl) diffraction lines for high-T_c, low-T_c ((Bi,Pb)2212) and Ca_2PbO_4 phases, respectively (see Fig. 3). When performing the calculation, the volume fractions of the (Bi,Pb)2223,

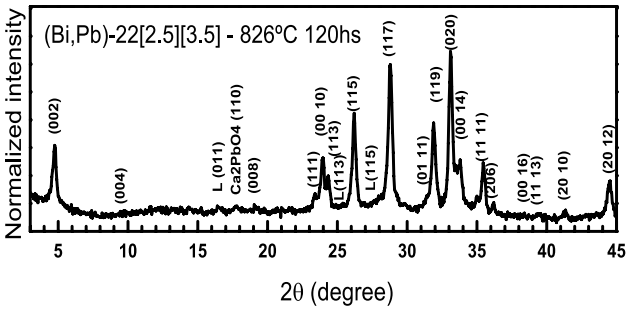

Fig. 3 X-ray diffraction pattern of powder samples before the last heat treatment. The reflections belonging to the (Bi,Pb)2212 and Ca_2PbO_4 phases are marked by "L" and "Ca_2PbO_4", respectively. The main peaks display their Miller's indexes

(Bi,Pb)2212 and Ca_2PbO_4 phases are estimated to be approximately 92, 6, and 2% respectively, for all samples. In the case of the (Bi,Pb)2223 phase, the unit-cell parameters were calculated assuming an orthorhombic unit cell and the obtained values $a = 5.3999$ Å, $b = 5.4037$ Å, and $c = 37.0762$ Å are in excellent agreement with those reported for the same compound elsewhere [16, 17].

Table 3 displays a summary of the microstructural properties of the three samples studied in this paper.

The effect of the compacting pressure has its fingerprint in the microstructure of these samples. This can be inferred from the fracture micrographs of samples MD2P1, MD2P2 and MD2P3 which are shown in Fig. 4a, b and c, respectively. In the micrographs it is observed that the granular morphology of three samples are similar, exhibiting grains with nearly platelet-like shape. Another observation also indicates changes in the sample porosity with increasing compacting pressures that correspond with the increase of the mass density.

The average grain size in the sample MD2P1 was found to be $L_a = (6.6 \pm 0.6)$ μm long and as thick as $L_c = (0.57 \pm 0.03)$ μm; for the sample MD2P2, the grains were found to have dimensions $L_a = (5.8 \pm 0.3)$ μm long and $L_c = (0.38 \pm 0.01)$ μm thick; in sample MD2P3 the grains have dimensions $L_a = (9.0 \pm 0.9)$ μm long and $L_c = (0.46 \pm 0.04)$ μm thick. The ratios L_a/L_c are shown in Table 3. These values have been found to be very sensitive to the compacting pressure and higher than those of 2.5 and 4.5 reported in $YBa_2Cu_3O_{7-\delta}$ ceramic samples [18], but similar

Table 3 Mass experimental density, d_r, volume fraction of pores and no-conductive phases, p, and shape anisotropy of the grains, L_a/L_c

Sample	d_r (g/cm^3)	p	L_a/L_c
MD2P1	4.60	0.269	11.6
MD2P2	4.98	0.209	15.4
MD2P3	5.20	0.173	19.6

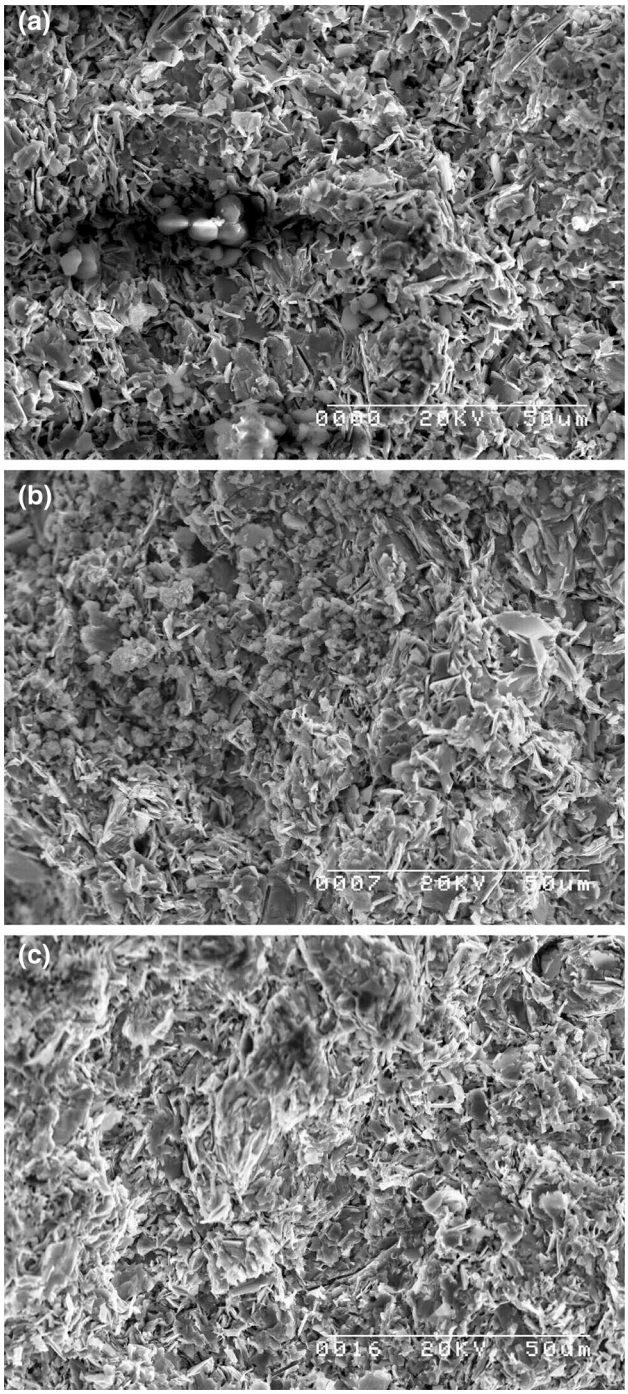

Fig. 4 Fracture micrographies of the samples obtained by SEM. **a** MD2P1, **b** MD2P2 and **c** MD2P3

to those estimated for both (Bi,Pb)2223 superconducting bulk and tapes [7, 19–21].

3.2 Electrical transport measurements

The experimental values are shown in Table 4. The parameters $\rho_x(0)$, $\rho_z(0)$, A_x and A_z, are obtained by linear fitting of the curves of electrical resistivity dependence with the temperature in the linear region at high temperatures. Here A_x, A_z are the slopes of the electrical resistivity and the $\rho_x(0)$, $\rho_z(0)$ the residual electrical resistivity in the two principal directions of the sample, respectively. This data is extracted from fittings in Fig. 5.

Figure 6 displays the way of determining the paracoherent resistivity, ρ_{px} of the samples. The ρ_{px} value is selected in the point where the straight line separates from ρ–J curve (see the inset in Fig. 6). The explanation of this method of selection was discussed in detail elsewhere [7, 9]. In addition, the MD2P1 sample shows the highest resistivity values at 103 K and the lowest intragranular critical current density of the sample set. The behavior of the samples compacted at higher pressures (MD2P2 and MD2P3) is similar for excitation current densities lower than their intragranular critical current density.

In Table 4 the external electric anisotropy, μ, has a minimum for the sample MD2P2 while the values of the orientation factor of the grain, f, decreases when the compacting pressure increases from 230 till 780 MPa. Such a decrease in f is mainly related with changes in grains shape as displayed in Table 3.

From the application of model described in reference [7] to our samples set, the main results are reported in Table 5. First, we have calculated the A_{ab} values by using two different expressions $A_x\alpha_{nx}$ and $A_z\alpha_{nz}$. However, the difference between the obtained values does not exceed 0.5% for each sample.

In addition, the calculated γ_{ab} can be approximated to 0.35 to all the samples even when the compacting pressures are quite different. This result justifies the low anisotropy at the level of the sample, $\mu \leq 1.46$.

Another relevant issue can be found when A_{ab} and ρ_{wl} of the samples are compared. As it is known, the presence of impurities of Ca_2PbO_4 (see X-ray pattern in Fig. 3), can purify the grain boundaries and strengthen the intergrain coupling [22, 23]. On the other hand, the increase of uniaxial compacting pressure can also improve the intergranular properties of the samples [19, 20]. The combination of these effects is the cause of the decrease in the weak links resistivity, ρ_{wl} (see Table 5). In addition, the reduction of A_{ab} parameter indicates an improvement in oxygenation degree [24] with increasing compacting pressures.

It very important to note that the sample MD2P2 exhibits also an abrupt fall in its effective intragranular anisotropy, t. At this point we would like to highlight that these results as compared with those obtained in samples with starting composition $Bi_{1.65}Pb_{0.35}Sr_2Ca_2Cu_3O_{10+\delta}$ [7] are different. The Ca, Cu enriched samples show an improvement in the electrical transport properties of the junctions reflected in a reduction of the weak links resistivity of 50% approximately, which agrees with the results obtained in reference [22].

Table 4 Slopes of the electrical resistivity at the sample level, A_x and A_z, residual electrical resistivities, $\rho_x(0)$ and $\rho_z(0)$, electrical resistivities at 300 K, ρ_x and ρ_z

Sample	Slope A_x (μΩ cm/K)	Slope A_z (μΩ cm/K)	$\rho_x(0)$ (mΩ cm)	$\rho_z(0)$ (mΩ cm)	$\rho_x(300)$ (mΩ cm)	$\rho_z(300)$ (mΩ cm)	μ (300 K)	ρ_{px} (mΩ cm)	f_x
MD2P1	5.600	7.960	0.856	1.311	2.535	3.704	1.46	0.177	0.207
MD2P2	3.350	4.200	0.430	0.555	1.432	1.808	1.26	0.079	0.183
MD2P3	4.080	5.670	0.506	0.717	1.729	2.416	1.40	0.071	0.139

All previous values were obtained in the two principal directions of the sample. Besides are shown the external electrical anisotropy, μ, the paracoherent resistivity in x-direction, ρ_{px}, and the orientation factor of the grains, f_x

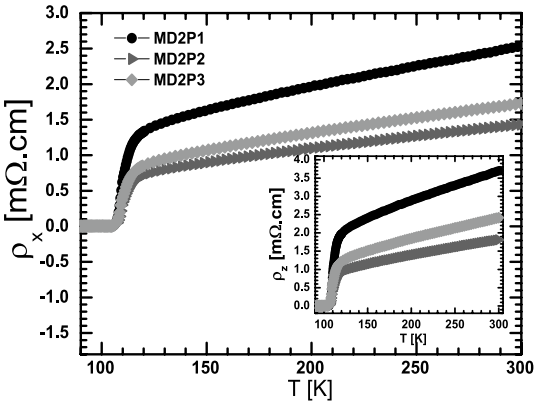

Fig. 5 Temperature dependencies of the resistivity tensor component, $\rho_x(T)$, of the samples MD2P1, MD2P2 and MD2P3. The inset shows the temperature dependencies of resistivity tensor component, $\rho_z(T)$, of the same samples. Some physical parameters extracted from $\rho_i(T)$ $i = x, z$ curves are displayed in Table 3 and discussed in the text

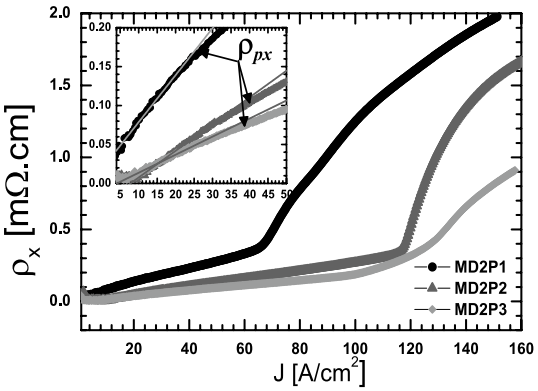

Fig. 6 The mean current density dependencies of x-axis resistivity, $\rho_x(J)$ for the samples MD2P1, MD2P2 and MD2P3, measured at constant temperature $T = 103$ K. The inset shows the measurement method to obtain the paracoherent resistivity, ρ_{px}

Also, a marked reduction of effective anisotropy of the grains is observed.

Finally we would like to comment the experimental results displayed in Fig. 7. Due to the way of cutting the samples and the location of the contacts in the Montgomery's method the effects of the thin layer of Bi-2212 phase normally detected in samples extracted from the top or bottom of the cylindrical pellet [7, 9] are not observed here. Note that in both directions x and z the resistivity of all the samples drops to zero essentially at the same temperature. The isotropic character of these samples also support the explanation of such behavior, since the probability of finding ab-planes is independent of the selected direction.

4 Conclusions

We have applied successfully the model described in reference [7] to estimate inter and intragranular magnitudes in samples measured by the Montgomery's method. The results show that the model works well in samples with low electrical anisotropy characterized by $\mu \sim 1$ and $\gamma_{ab} \sim 0.33$. Even when the results agree with the case of granular random misalignment, the values of intrinsic effective anisotropy t decrease in one magnitude order with the compacting pressure. This behaviour also was found in samples with $\mu > 1$ and $\gamma_{xa} > 0.33$ [7, 9].

The main effects of the Ca, Cu enriched environment in the synthesis of (Bi–Pb)-2223 phase are the reductions of the weak links resistivity, of the electrical anisotropy of the grain and of the sintering temperature. The obtained samples have ~ 92% of the (Bi–Pb)-2223 phase.

A compacting pressure of 488 MPa optimizes the inter and intragranular transport properties of the (Bi–Pb)-2223 ceramic samples obtained under the conditions mentioned above.

The results presented in this paper and other published [9], strongly suggest that the excess of Ca and Cu

Table 5 Outputs parameters of the model described in reference [7]

Sample	γ_{xa}	t	α_{nx}	α_{nz}	$A_{ab} = A_x\alpha_{nx}$ (μΩ cm/K)	$A_{ab} = A_z\alpha_{nz}$ (μΩ cm/K)	ρ_{wlx} (mΩ cm)	ρ_{wlz} (mΩ cm)
MD2P1	0.3523	44,522	0.134	0.092	0.752	0.751	0.115	0.120
MD2P2	0.3474	697	0.133	0.106	0.447	0.444	0.057	0.059
MD2P3	0.3512	1632	0.108	0.077	0.441	0.438	0.055	0.055

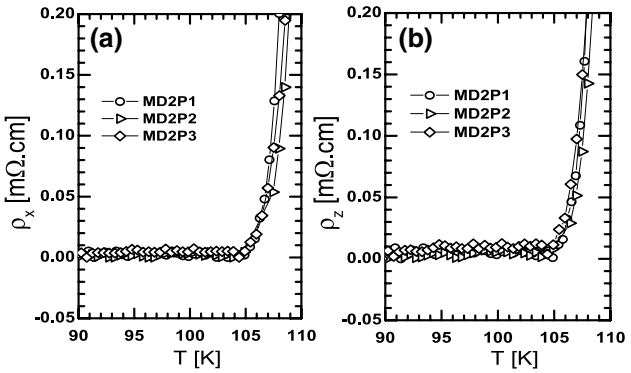

Fig. 7 $\rho_i(T)$ (with $i = x, z$) dependencies in the two main directions for the three samples studied in this article

combined with compacting pressure in (Bi–Pb)-2223, can be used to improve the electrical transport performance in (Bi–Pb)-2223 ceramic samples. However, such issue has been poorly discussed in the literature [22].

Acknowledgements This work was partially supported by CAPES/MES-CUBA, Project 104/10. We thank the support of R. Packard (University of California at Berkeley) and all the help by F. Calderón-Piñar and O. García-Zaldivar (Group of Ferroelectricity and Magnetism, IMRE-Physics Faculty, University of Havana).

References

1. E. Govea-Alcaide, M. Hernández-Wolpez, A.J. Batista-Leyva, R.F. Jardim, P. Muné, Physica C **423**, 51–56 (2005)
2. H. C. Montgomery, J. Appl. Phys. **42**, 2971–2975 (1971)
3. B.F. Logan, S.O. Rice, R.F. Wick, J. Appl. Phys. **42**, 2975–2980 (1971)
4. L.J. van der Pauw, Philips Res. Rep. **16**, 187–195 (1961)
5. D. Wasscher, Philips Res. Rep. **16**, 301–306 (1961)
6. C.A.M. dos Santos, A. de Campos, M.S. da Luz, B.D. White, J.J. Neumeier, B.S. de Lima, C.Y. Shigue. J. Appl. Phys. **110**, 083703 (2011)
7. A. Cruz-García, E. Altshuler, J.R. Fernández-Gamboa, R.F. Jardim, O. Vázquez-Robaina, P. Muné, J. Mater. Sci. Mater. Electron. **28**, 13058–13069 (2017)
8. A. Cruz-García, P. Muné, Physica C **527**, 74–79 (2016)
9. A. Cruz-García, J.R. Fernández-Gamboa, E. Altshuler, R.F. Jardim, O. Vazquez-Robaina, P. Muné, J. Mater. Sci. Mater. Electron. **29**, 6188–6199 (2018)
10. P. Muné, E. Govea-Alcaide, R.F. Jardim, Physica C **384**, 491–500 (2003)
11. X. Yang, T.K. Chaki, Supercond. Sci. Technol. **6**, 343–348 (1993)
12. K. Kocabaş, M. Gökçe, M. Çiftçioğlu, Ö. Bilgili, J. Supercond. Nov. Magn. **23**, 397–410 (2010)
13. P. Villars, K. Cenzual, *Pearson's Crystal Data: Crystal Structure Database for Inorganic Compounds (on CD-ROM), Version 1.0, Release 2007/8* (ASM International, Materials Park, 2007)
14. C.W. Chiu, R.L. Meng, L. Gao, Z.J. Huang, F. Chen, Y.Y. Xue, Nature **365**, 323–325 (1993)
15. S.A. Halim, S.A. Khawaldeh, S.B. Mohammed, H. Azhan, Mater. Chem. Phys. **61**, 251–259 (1999)
16. S. Safran, A. Kılıç, O. Ozturk, J. Mater. Sci. Mater. Electron. **28**, 1799–1803 (2016)
17. D. Pandey, R. Mahesh, A.K. Singh, V.S. Tiwari, Physica C **184**, 135–143 (1991)
18. A. Díaz, J. Maza, F. Vidal, Phys. Rev. B **55**, 1209–1215 (1997)
19. E. Govea-Alcaide, P. Muné, R.F. Jardim, Braz. J. Phys. **35**, 680–688 (2005)
20. E. Govea-Alcaide, R.F Jardim, P. Muné, Phys. Stat. Sol. **13**, 2484–2493 (2005)
21. T.T. Tan, S. Li, H. Cooper, W. Gao, H.K. Liu, S.X. Dou, Supercond. Sci. Technol. **14**, 471–478 (2001)
22. V.S. Kravtchenko, M.A. Zhuravleva, Y.M. Uskov, O.G. Potapova, N.A. Bogoljubov, P.P. Bezverkhy, L.L. Makarshin, Superlattices Microstruct. **21**, 87–94 (1997)
23. D. Shi, M.S. Boley, U. Welp, J.G. Chen, Y. Liao, Phys. Rev. **40**, 5255–5258 (1989)
24. T. Fujii, T. Watanabe, A. Matsuda, Physica C **357–360**, 173–176 (2001)